Accepted Manuscript
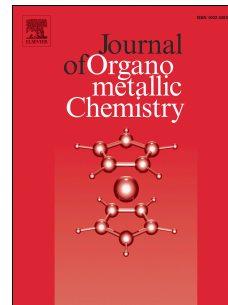
Complex formation between $[(\eta^6\text{-}p\text{-cym})Ru(H_2O)_3]^{2+}$ and oligopeptides containing three histidyl moieties

Zsolt Bihari, Valeria Ugone, Eugenio Garribba, Norbert Lihi, Péter Buglyó

Please cite this article as: Z. Bihari, V. Ugone, E. Garribba, N. Lihi, P. Buglyó, Complex formation between $[(\eta^6\text{-}p\text{-cym})Ru(H_2O)_3]^{2+}$ and oligopeptides containing three histidyl moieties, *Journal of Organometallic Chemistry* (2016), doi: 10.1016/j.jorganchem.2016.09.013.
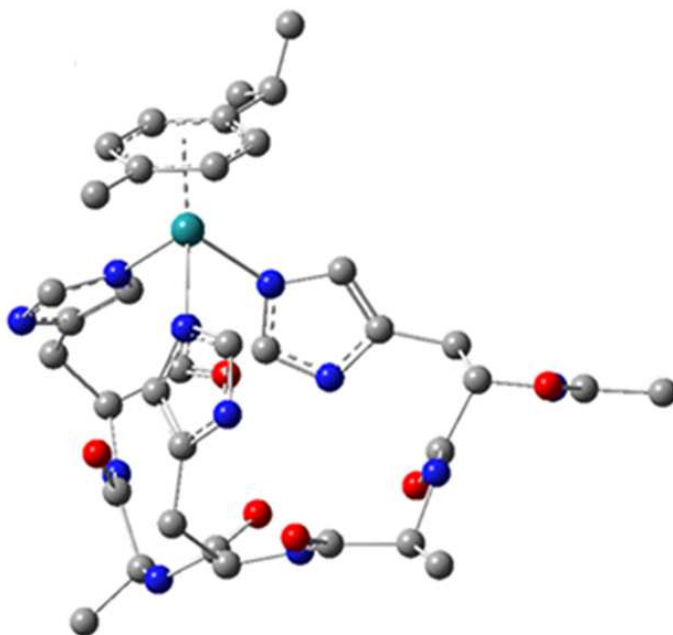
Supported by DFT calculations, formation of stable mononuclear ($N1_{\text{Im}}$, $N1_{\text{Im}}$, $N1_{\text{Im}}$) coordinated complexes was found in the $[\text{Ru}(\eta^6\text{-}p\text{-cym})(\text{H}_2\text{O})_3]^{2+}$–Ac-HAHH-NH$_2$ or –Ac-HAHAH-NH$_2$ systems in slow processes to model the metal ion binding capabilities of surface-accessible histidyl imidazoles of albumin and transferrin.

Complex formation between [(η^6-*p*-cym)Ru(H$_2$O)$_3$]$^{2+}$ and oligopeptides containing three histidyl moieties

Zsolt Bihari [a], Valeria Ugone [b], Eugenio Garribba [b], Norbert Lihi [a] and Péter Buglyó [a,*]

[a] Department of Inorganic and Analytical Chemistry, University of Debrecen, H-4032 Debrecen, Hungary
[b] Department of Chemistry and Pharmacy, University of Sassari, Via Vienna 2, I-07100 Sassari, Italy

Abstract

In order to model the metal ion binding capabilities of high molecular mass components of blood the interaction between [(η^6-*p*-cym)Ru(H$_2$O)$_3$]$^{2+}$ and terminally protected oligopeptides containing three histidyl moieties (Ac-HHH-NH$_2$, Ac-HAHH-NH$_2$, Ac-HAHAH-NH$_2$ and Ac-H*AH*AH*-NH$_2$, where A = L-alanyl, H = L-histidyl, H* = *N3*-methyl-L-histidyl) were studied by pH-potentiometric, ESI-TOF-MS, circular dichroism and NMR methods at an ionic strength of 0.20 M KCl or KNO$_3$ as well as using density functional theory (DFT) calculations. Protonation constants of the novel peptides are reported. Although for Ac-HHH-NH$_2$ the immediate formation of precipitation with [(η^6-*p*-cym)Ru(H$_2$O)$_3$]$^{2+}$ hindered any further solution investigations results of the detailed NMR and MS studies revealed that the other three ligands coordinate to the metal ion in rather slow processes via the imidazole moieties forming [(η^6-*p*-cym)RuL]$^{2+}$ (L = oligopeptide) type species in the slightly acidic, neutral pH-range. At pH ~ 7.5 identical binding mode of Ac-HAHH-NH$_2$ and Ac-HAHAH-NH$_2$ in the [(η^6-*p*-cym)RuL]$^{2+}$ via three imidazole nitrogens was found hindering completely the hydrolysis of the metal ion even at 1:1 metal ion to ligand ratio. At elevated pH MS evidences support the involvement of amide-N donor(s) in metal ion binding too beside partial hydrolysis. 0.20 M KCl medium was found to hinder effectively the hydrolytic processes of the metal ion in the basic pH-range without altering the coordination of the imidazole side chains. Both NMR and DFT results support the imidazole-*N1* („far" or „τ") over the *N3* („near" or „π") coordination of the histidyl side chains of all these oligopeptides to the organometallic ruthenium(II) cation.

1. Introduction

The biologically active low oxidation state of various platinum metals with antiproliferative potential can be stabilized in half-sandwich type [(η^6-arene)M(XY)Z] (M = Ru(II), Os(II)) and [(η^5-Cp)M(XY)Z] (Cp = substituted cyclopentadienyl; M = Rh(III), Ir(III),

XY = chelator, Z = monodentate ligand) organometallic complexes. In blood serum these compounds may undergo various biotransformation reactions. As the histidyl residue of peptides possesses a very efficient, either „far" or „τ" (*N1*) as well as „near" or „π" (*N3*) nitrogen donor (see Scheme 1) in its side chain imidazole ring [1], surface-accessible histidyl imidazoles of albumin and transferrin (e.g. 38 histidyl residues available in apo-Tf) are important metal ion sites. It is widely accepted that these proteins have determining role in the uptake of platinum compounds therefore these interactions will determine the overall drug distribution and excretion and differences in efficacy, activity and toxicity [2]. Studies, therefore, involving the binding of imidazole, histidine or histidyl side chains to various metal ions are in the focus of intensive research [3-9].

Scheme 1.

Ruthenium compounds as a possible alternative to anticancer platinum complexes often selectively coordinate histidyl imidazole nitrogens on proteins and the *N7* site on the imidazole ring of purine nucleotides, and so can take advantage of the properties of proteins, oligonucleotides and nucleic acids to target specific tissues [10,11]. As expected on the basis of the relative pK_a of the ligands, ruthenium binding to imidazoles on protein surfaces is greater than to guanine *N7* on DNA [1]. Such interactions could be responsible for drug inactivation (related to resistance) or activation (e.g. in the case of prodrugs) and drug delivery.

For a better understanding of the interaction between organometallic, half-sandwich type platinum metals and surface-accessible histidyl imidazoles of peptides in serum, previously the $[(\eta^6\text{-}p\text{-cym})Ru(H_2O)_3]^{2+}$ binding strength of N-methylimidazole was studied [12]. In particular, by the combined use of potentiometry, NMR and mass spectrometry (MS) we have shown that even this simple model ligand forms complexes with high stability with $[(\eta^6\text{-}p\text{-cym})Ru(H_2O)_3]^{2+}$ and can hinder its hydrolysis under physiologically relevant conditions at 1:3 metal ion to ligand ratio [12].

Due to tautomerization in the imidazole ring of the histidyl side chain both the *N1* and *N3* nitrogen donors can coordinate to the metal ions; under special conditions imidazolato-bridged dinuclear complexes can also be obtained [13,14]. In reactions of palladium(II) with histidyl peptides having free N-terminus, imidazole *N3* coordination is preferred due to the [NH$_2$, *N3*$_{Im}$] „histamine-type" binding of the ligands [14,15]. On the contrary, previously reported oligopeptides with protected N-terminus (Ac-HAAAH-NH$_2$ and Ac-HARAH-NH$_2$) can bind to metal ions (M = $[Pd(en)(H_2O)_2]^{2+}$ and *cis*-$[Ru(NH_3)_4]^{2+}$) through imidazole *N1* or

2

N3 of either histidine, thereby potentially forming linkage isomers, [M{1,5-Ac-H(*N1*)-(Xaa)$_3$-H(*N1*)-NH$_2$}]$^{2+}$, [M{1,5-Ac-H(*N1*)-(Xaa)$_3$-H(*N3*)-NH$_2$}]$^{2+}$, [M{1,5-Ac-H(*N3*)-(Xaa)$_3$-H(*N1*)-NH$_2$}]$^{2+}$ and [M{(1,5-Ac-H(*N3*)-(Xaa)$_3$-(*N3*)-NH$_2$}]$^{2+}$, resulting in 20-22-membered macrocycles [16-18]. Using ^{13}C NMR spectroscopy for assignment, the differences between δ_C for each imidazole-C atoms (C2, C4 and C5) of the complexed and those of the free peptide assisted in identifying the structure of each possible isomers [19]. To simplify the chemistry, the number of linkage isomers was reduced by using *N3*-methylated histidines too, leaving only *N1* for binding. It was shown by ^{13}C NMR that *N1* coordination of both of the His residues resulted in negative $\Delta\delta$ for C4 and positive $\Delta\delta$ values for the C5 atoms [16-19].

In continuation of our work, further studies on the interaction between [(η^6-*p*-cym)Ru(H$_2$O)$_3$]$^{2+}$ and model peptides containing histidyl residues in various positions were undertaken. His-rich peptides e.g. HRP2 may be important targets for the development of novel antimalarial tests while histidine triad proteins (HIT) containing highly conserved HXHXH sequence by binding purine mono-nucleotides are shown to be involved in proapoptotic tumor suppression [20,21]. In the present work we report on the synthesis and results obtained with the ruthenium(II) complexes of terminally protected peptides containing three histidyl residues in different sequences (Ac-HHH-NH$_2$, Ac-HAHH-NH$_2$, Ac-HAHAH-NH$_2$ and Ac-H*AH*AH*-NH$_2$, where H* = *N3*-methyl-L-histidyl, Fig. 1). Beside the detailed equilibrium study carried out by the combined use of pH-potentiometric, NMR, CD and ESI-MS techniques in aqueous solution, DFT methods were also used to calculate the optimized structures and the most stable isomers of the complexes formed at physiological pH. To model the biologically more relevant conditions the studies were also extended to a medium containing 0.20 M KCl ionic strength.

Fig. 1

2. Materials and methods

2.1. Chemicals

RuCl$_3$·xH$_2$O, α-terpinene, AgCF$_3$SO$_3$, AgNO$_3$, KNO$_3$ and KCl were commercial products of the highest purity available (Sigma-Aldrich, Merck or VWR), and used as received. Solvents were dried and distilled according to standard methods [22]. [(η^6-*p*-cym)RuCl$_2$]$_2$ was synthesized and purified according to a literature protocol [23]. Aqueous solution of [(η^6-*p*-cym)Ru(H$_2$O)$_3$](NO$_3$)$_2$ was obtained from [(η^6-*p*-cym)RuCl$_2$]$_2$ by removal of chloride ion using equivalent amount of AgNO$_3$ [24]. The N- and C-terminally protected

peptides with the sequence of Ac-His-His-His-NH$_2$ (HHH), Ac-His-Ala-His-His-NH$_2$ (HAHH), Ac-His-Ala-His-Ala-His-NH$_2$ (HAHAH) and Ac-His(*N3*-Me)-Ala-His(*N3*-Me)-Ala-His(*N3*-Me)-NH$_2$ (H*AH*AH*) (see Fig. 1) were obtained by solid-phase peptide synthesis using the Fmoc strategy. Rink Amide AM resin, TBTU and Fmoc-protected L-amino acids (Fmoc-L-His(Trt)-OH, Fmoc-L-Ala-OH) were purchased from Novabiochem (Switzerland) and from Chem-Impex International Inc. (USA). N,N-diisopropyl-ethylamine (DIPEA), trifluoroacetic acid and analytical grade dimethylformamide (DMF) were Merck products. 3,6-dioxa-1,8-octanedithiol (DODT), N-methyl-pyrrolidone (NMP), 1-hydroxybenzotriazole hydrate (HOBt·H$_2$O), triisopropylsilane (TIS), 2-methyl-2-butanol and HPLC grade trifluoroacetic acid were supplied by Sigma-Aldrich. Dichloromethane (DCM), diethyl ether (Et$_2$O), acetic acid, piperidine, acetic anhydride and acetonitrile (ACN) were purchased from Molar or VWR.

2.2. Synthesis and physical measurements

2.2.1. Peptide synthesis and purification

The histidine-containing oligopeptides were synthesized by solid-phase peptide synthesis in a microwave-assisted Liberty 1 Peptide Synthesizer (CEM, Matthews, NC), using the TBTU/HOBt/DIPEA activation strategy on Rink Amide AM resin (substitution 0.71 mmol·g^{-1}, 0.25 mmol·g scale, 352 mg of resin). Removal of the Fmoc group was carried out by means of 20% piperidine/0.1 M HOBt·H$_2$O in DMF at 75 °C with 35 watts microwave power for 180 s. 0.5 M HOBt·H$_2$O/0.5 M TBTU in DMF and 2 M DIPEA in NMP were used for coupling at 75 °C with 25 watts microwave power for 300 s, adding 4-fold excess of amino acids (except for the coupling of Fmoc-L-His(*N3*-Me)-OH, where 2.5 equivalents of amino acid was used). The N-terminal Fmoc group was removed as described above. N-terminal acetylation was achieved by treating the fully assembled peptide resin with capping reagents (5% Ac$_2$O, 6% DIPEA in DMF). Histidines were protected with trityl (Trt) groups during the peptide assembly. Cleaving from the resin and removal of the side chain protective groups were carried out by treatment with a mixture containing TFA/TIS/H$_2$O/DODT (94/2.5/2.5/1 v/v %) at room temperature for 1.5 h. After cleaving, the free peptide was separated from the resin by filtration. Cold Et$_2$O was used to precipitate the crude peptides from the solution and to wash from the contaminants of the reagents of the synthesis and cleaving agents. After filtering, the product was dried under argon, redissolved in water and lyophilized.

In order to check the purity of the peptides analyses were performed using a Jasco analytical RP-HPLC instrument, equipped with a Jasco MD-2010 plus multi-wavelength detector on a Vydac C18 chromatographic column (250 x 4.6 mm, 300 Å pore size, 5 μm particle size). By eluting A solvent (0.1% TFA in water) and B solvent (0.1% TFA in ACN) at a flow rate of 1 ml/min the absorbance at 222 nm was monitored. Method A: 30 min 98% A and 2% B (isocratic), method B: 3 min 100% A and 0% B (isocratic), 15 min 90% A and 10% B (gradient), 18 min 90% A and 10% B (isocratic), 20 min 100% A and 0% B (gradient). Purity of the peptides (> 95%) was checked by analytical RP-HPLC and the protonation sites were identified by pH-potentiometric measurements. ESI-TOF MS analysis in the positive mode was carried out on a Bruker micrOTOF-Q instrument. The measurements were performed in water, in the absence or presence of chloride ions at 1.0 mM $[(\eta^6\text{-}p\text{-}cym)Ru(H_2O)_3]^{2+}$ concentration using different pH values. Temperature of drying gas (N_2) was 180 °C. The pressure of the nebulizing gas (N_2) was 0.3 bar. The flow rate was 3 μL/min. The spectra were accumulated and recorded by a digitalizer at a sampling rate of 2 GHz. DataAnalysis (version 3.4) was used for the calculation.

[Ac-HHH-NH$_2$](CF$_3$COO)$_3$: R_t = 3.89 min (method A). Yield: 20.7%. ESI-MS (pos.) m/z: 157.744 $[M - 3\ CF_3COO]^{3+}$, calc. for $[M - 3\ CF_3COO]^{3+}$: 157.745; 236.108 $[M - 3\ CF_3COO - H]^{2+}$, calc. for $[M - 3\ CF_3COO - H]^{2+}$: 236.114; 471.219 $[M - 3\ CF_3COO - 2\ H]^+$, calc. for $[M - 3\ CF_3COO - 2H]^+$: 471.221.

[Ac-HAHH-NH$_2$](CF$_3$COO)$_3$: R_t = 4.24 min (method A). Yield: 46.5%. ESI-MS (pos.) m/z: 181.425 $[M - 3\ CF_3COO]^{3+}$, calc. for $[M - 3\ CF_3COO]^{3+}$: 181.424; 271.632 $[M - 3\ CF_3COO - H]^{2+}$, calc. for $[M - 3\ CF_3COO - H]^{2+}$: 271.633; 542.263 $[M - 3\ CF_3COO - 2\ H]^+$, calc. for $[M - 3\ CF_3COO - 2\ H]^+$: 542.258.

[Ac-HAHAH-NH$_2$](CF$_3$COO)$_3$: R_t = 5.54 min (method A). Yield: 57.4%. ESI-MS (pos.) m/z: 205.104 $[M - 3\ CF_3COO]^{3+}$, calc. for $[M - 3\ CF_3COO]^{3+}$: 205.103; 307.151 $[M - 3\ CF_3COO - H]^{2+}$, calc. for $[M - 3\ CF_3COO - H]^{2+}$: 307.151; 613.297 $[M - 3\ CF_3COO - 2\ H]^+$, calc. for $[M - 3\ CF_3COO - 2\ H]^+$: 613.295.

[Ac-H*AH*AH*-NH$_2$](CF$_3$COO)$_3$: R_t = 11.1 min (method B). Yield: 39.5%. ESI-MS (pos.) m/z: 219.116 $[M - 3\ CF_3COO]^{3+}$, calc. for $[M - 3\ CF_3COO]^{3+}$: 219.119; 328.171 $[M - 3\ CF_3COO - H]^{2+}$, calc. for $[M - 3\ CF_3COO - H]^{2+}$: 328.175; 655.341 $[M - 3\ CF_3COO - 2\ H]^+$, calc. for $[M - 3\ CF_3COO - 2\ H]^+$: 655.343.

2.2.2. pH-potentiometry

For solution studies doubly deionised and ultra-filtered water was obtained from a Milli-Q RG (Millipore) water purification system. pH-potentiometric measurements were carried out at an ionic strength of 0.20 M KNO_3 or 0.20 M KCl and at 25.0 ± 0.1 ^{o}C. Carbonate-free KOH solutions of known concentrations (*ca.* 0.2 M) were used as titrant. HNO_3 or HCl stock solutions (*ca.* 0.2 M) were prepared from concentrated nitric or hydrochloric acids, respectively, and the exact concentrations were determined by potentiometric titrations using the Gran's method [25]. A Mettler Toledo T50 titrator equipped with a Metrohm double junction electrode (type 6.0255.100) or a combined glass electrode (type 6.0234.100) was used for the pH-metric measurements. The electrode system was calibrated according to Irving et al. [26], the pH-metric readings could therefore be converted into hydrogen ion concentrations. The water ionization constant, pK_w, was 13.76 ± 0.01. For the metal ion containing samples automatic titrations with a maximum waiting time of 30 minutes in every step were performed in the pH range 2.0–11.0 using samples of 6.00 mL. In all cases the samples were completely deoxygenated by bubbling purified argon for *ca.* 20 min before the measurements. Owing to slow equilibrium processes individual samples containing the metal ion and ligand in 1:1 ratio were also prepared in vials under an atmosphere of argon using 0.20 M KNO_3 ionic strength. The samples were left to stand for 7 days and the pH values were measured in the absence of CO_2 from the air. Metal ion concentrations in all cases were varied in the range 1.0–5.0 mM. Concentration stability constants, $\beta_{p,q,r} = [M_pL_qH_r]/[M]^p[L]^q[H]^r$ (where "M" stands for $[(\eta^6\text{-}p\text{-cym})Ru(H_2O)_3]^{2+})$ were calculated with the aid of the SUPERQUAD and PSEQUAD computer programs [27,28]. During the calculations hydrolysis of $[(\eta^6\text{-}p\text{-cym})Ru(H_2O)_3]^{2+}$ was taken into consideration and the formation of the following species was assumed: $[\{(\eta^6\text{-}p\text{-cym})Ru\}_2(\mu^2\text{-}OH)_3]^+$ ($\log\beta_{2,0,-3} = -9.16$) [29].

2.2.3. Spectroscopic measurements

A JASCO J-810 spectropolarimeter was used to record the CD spectra of the complexes in the wavelength range of 200 to 800 nm using a 10 mm cell. Individual Ru-containing samples at $c_{Ru} = 1.0$ mM were equilibrated in H_2O for 7 days before measurements.

The NMR spectra (^1H, ^{13}C, ^1H-^1H COSY, ^1H-^1H NOESY, ^1H-^{13}C HSQC, ^1H-^{13}C HMBC) were recorded on a Bruker Avance DRX 400 FT-NMR instrument. 2D NOESY experiment was carried out with a standard pulse sequence combined with gradient pulses in

6

mixing time. In the experiments 800 ms mixing time (d8) was used to allow time for magnetization exchange to occur for the NOE interactions. Chemical shifts are reported in ppm (δ_H) from sodium 3-(trimethylsilyl)-propionate (TSP) as internal reference. NMR studies were carried out in D_2O (99.8%) at c_{Ru} = 5.0–10.0 mM in order to register the pH* dependence of the chemical shifts of the nuclei of various species. pH* was set up with NaOD, DNO_3 or DCl in D_2O. Individual Ru-containing samples were equilibrated for 7 days before measurements. pH* values (direct pH-meter readings in a D_2O solution of a pH-meter calibrated in H_2O according to Irving et al. [26] were converted to pH values measurable at an ionic strength of 0.20 M using the following equation: pH = pH* + 0.40 [30].

2.3. Density functional theory (DFT) calculations

Geometries were fully optimized by DFT using the Gaussian 09 (revision C.01) software [31]. According to previous studies [32,33] the functional B3P86 was used which ensures a high degree of accuracy in the prediction of the structures of transition metal complexes [34]. The relativistic small-core ECPs SDD (the Stuttgart-Dresden ECP) [35] and LANL2DZ [36] with the corresponding valence basis sets were employed on the ruthenium, and 6-311g on the ligand. For all the structures, minima were verified through a frequency calculation. The closed-shell Ru species were treated with the restricted formalism. The relative free energy of the several isomers and conformations of the ML complexes were calculated at the level of theory B3P86/6-311g by computing the solvent (in this study, water) effect using the SMD model available in Gaussian 09 software. The SMD model is based on the quantum mechanical charge density of a solute molecule interacting with a continuum description of the solvent, which takes into account the full solute electron density without defining partial atomic charges and represents the solvent not explicitly but rather as a dielectric medium with surface tension at the solute-solvent boundary. This model has been demonstrated to give good results in the prediction of solvation free energy [37]. The total value of ΔG^{tot}_{aq} can be separated into the electronic plus nuclear repulsion energy (ΔE^{ele}), the thermal contribution (ΔG^{therm}) and the solvation free energy ($\Delta(\Delta G^{solv})$): $\Delta G^{tot}_{aq} = \Delta E^{ele} + \Delta G^{therm} + \Delta(\Delta G^{solv})$. The thermal contribution was estimated by using the ideal gas model and the calculated harmonic vibrational frequencies to determine the correction arising from zero point energy and the thermal population of the vibrational levels. The theory was described in the literature [38-42].

3. Results and discussion

3.1. Characterization of the peptide ligands

As it was detailed in the Experimental section the novel oligopeptides were obtained via conventional solid-phase peptide synthesis. The crude products were purified via RP-HPLC. A typical chromatogram is shown in Fig. S1 and indicated (as for the other ligands too) > 95% purity. Identity of the peptides was assessed by HR-ESI-MS and pH-potentiometry. Evaluation of the titration curves (for a representative example, see Fig. S2) resulted in protonation constants of the ligands summarized in Table 1. The number and the numerical value of the pK data are both consistent with the presence of three imidazole moieties in each of the peptides providing thus further proof for the identity of them. The values are in the range 5.6–7.0 characteristic for the protonation of the histidyl moieties of small peptides [43]. The slightly increasing value of pK_1 in the direction of HHH → HAHAH may be interpreted with the decreasing strength of H-bonding between the imidazole units due to the increasing size of the chelate that is formed in the doubly protonated ligands.

Table 1.

pH-dependent ^{1}H NMR study of peptide ligands (as an example see HAHAH in Fig. 2) indicates that the Hε_1 (□) and Hδ_2 (○) protons of the imidazolyl moieties exhibit the largest upfield shift with increasing pH of the samples. COSY and HMBC experiments (Fig. S3) assisted in identifying the corresponding resonances belonging to the δ_2 and ε_1 protons of the imidazole rings. The chemical shift values registered for the fully protonated and fully deprotonated forms of HAHH and HAHAH are summarized in Table 2.

Fig. 2

Table 2

3.2. Complex formation of the ligands with $[(\eta^6\text{-}p\text{-cym})Ru(H_2O)_3]^{2+}$

Interaction between the His-containing novel peptides and $[(\eta^6\text{-}p\text{-cym})Ru(H_2O)_3]^{2+}$ was studied using pH-potentiometry. For HHH the formation of a yellow precipitate as low as pH = 2.0 and the very limited solubility of the complex(es) even at elevated pH hindered subsequent solution equilibrium studies with this ligand. For the tetrapeptide and pentapeptide slow complex formation processes were detected, 30 minutes waiting time being not enough to reach pH eqilibrium as it is shown in Fig. S2, curve b. Nevertheless, the titration curve in

Fig. S2 clearly shows that in the presence of the metal ion the complex formation is significant by pH 4 as cooperative deprotonation and coordination of two imidazole units is detectable. A further base consumption process by pH 8 is consistent with the binding of the third imidazole group of the ligand while above pH 9 hydrolysis of the complex(es) present is indicated. Due to the non-equilibrium processes, however, no attempts were made to calculate stability constants for the metal complex(es) present in solution from the pH-potentiometric curves in neither of the systems.

pH-dependence of the aromatic region of ^{1}H NMR spectra of equilibrated samples containing 1:1 metal ion to ligand ratio for the HAHAH system are presented in Fig. 3. As it can be seen in Fig. 3 at pH 2.17 beside the two doublets (Δ, 5.73 and 5.98 ppm) belonging to the ring protons of the *p*-cymene unit of the aqua complex, $[(\eta^6\text{-}p\text{-cym})Ru(H_2O)_3]^{2+}$ (for notation see Scheme 1) [29], resonances of the ε_1 protons (□, 8.63 ppm) and those of the δ_2 protons (○, 7.32 ppm) of the uncomplexed ligand are present. On increasing the pH, small new signals as low as pH 2.6 are detectable next to the above mentioned resonances indicating complex formation. This becomes more pronounced around pH 4 (suggesting binding isomers) and at pH 7.82 all the signals present unambiguously support the formation of a single complex (Hε_1: ●, Hδ_2: ■, *p*-cymene: ▲). Beside this species at more basic pH minor hydrolysis of the metal ion resulting in the formation of $[\{(\eta^6\text{-}p\text{-cym})Ru\}_2(\mu^2\text{-OH})_3]^+$ (Δ, 5.17 and 5.38 ppm) [29] and presence of some uncomplexed ligand (□, 7.64 and ○, 6.90 ppm) are also detected.

Fig. 3

It is also worth mentioning that the solution equilibrium studies carried out under biologically more relevant conditions, i.e. in the presence of 0.20 M KCl ionic strength, indicated that chloride ions are capable of hindering significantly the hydrolysis of the metal ion. To illustrate this, comparison of the pH-dependence of the ^{1}H NMR spectra for the $[(\eta^6\text{-}p\text{-cym})Ru(H_2O)_3]^{2+}$–HAHH system at 0.20 M KNO$_3$ or KCl are shown in Fig. S4.

In order to assign all the resonances for the new complex at pH 7.82 ^{1}H–^{1}H COSY (Fig. 4), ^{1}H–^{13}C HSQC (Fig. 5) and ^{1}H-^{1}H NOESY (Fig. S5) experiments were carried out. Fig. 4 clearly indicates the correlation between the corresponding ε_1 signals (■) and δ_2 signals (●); the assigned resonances together with chemical shift values are summarized in Table 2. As Fig. 5 demonstrates, the signals in the ppm range 6.1–5.6 involve the *p*-cymene ring carbons at 85–90 ppm while two C5 imidazole ring carbons out of the three ones appear at ~

128 ppm. The third C5–Hδ_2 crosspeak can be seen at 7.2 ppm in ^{1}H NMR spectrum, while the three C2 signals are detectable in the range 140–145 ppm in the ^{13}C NMR spectrum. The NOESY spectrum (Fig. S5) also shows that there is a through-space correlation between all the Im protons (ϵ_1, δ_2) and *p*-cym ring protons revealing the coordination of all the three Im units. All these data together with the absence of any uncomplexed ligand clearly support that at pH 7.8 a single species with (N$_{Im}$, N$_{Im}$, N$_{Im}$) coordination is present with HAHAH and with HAHH (Fig. S4) too.

Fig. 4.

Fig. 5.

As it is seen in Fig. 3, above pH 7.8 upfield shift of the aromatic resonances belonging to the complex can be seen (similar trends are also observable for the [(η^6-*p*-cym)Ru(H$_2$O)$_3$]$^{2+}$–HAHH system) that indicates change in the coordination sphere of the metal ion. This can either be partial hydrolysis during which the imidazole(s) are replaced by hydroxide ions or metal ion assisted deprotonation and coordination of the amide group(s) of the peptides. Although the high field region of the spectra (not shown) are less informative due to the presence of numerous overlapping CH$_2$ and CH signals and the disturbing water signal, comparison of these resonances in the absence and presence of the metal ion may also indicate some shift in accordance with literature data [44-47] suggesting amide coordination. Furthermore, the fact that even above pH 11 in both systems a significant amount of the metal ion can be found in complexed form may also suggest that hydrolysis can be ruled out. In order to obtain more information CD spectroscopy and ESI-MS techniques were also applied.

Selected CD spectra aquired in the range 2.2 < pH < 7.5 for the [(η^6-*p*-cym)Ru(H$_2$O)$_3$]$^{2+}$–tetrapeptide and –pentapeptide systems are shown in Fig. 6/A. As it is expected (not shown in Fig. 6) [(η^6-*p*-cym)Ru(H$_2$O)$_3$]$^{2+}$ or [{(η^6-*p*-cym)Ru}$_2$(μ^2-OH)$_3$]$^+$ ions do not exhibit CD activity. Since coordination of a chiral ligand to the half-sandwich type metal core results in the formation of a stereogenic metal center CD activity in the VIS part of the spectrum can also be expected [48]. Spectra belonging to the two metal ion containing systems already at pH 2.2 show a positive Cotton-effect at ~ 400 nm indicating complex formation in agreement with the NMR results. Around pH 4 an increase of the CD activity together with a bathochromic shift is detected (Fig. 6/A spectra c and d) in both systems providing support for the likely formation of binding isomers (see Fig. 3, pH = 4.26; Fig. S4B, pH 4.67). Around physiological pH where a single complex was detected in both

10

systems by NMR the CD spectra (Fig. 6/A spectra e and f) have positive Cotton-effect at ca. 300 and 370 nm different from those observed at pH 4. The similar pairs of CD spectra at various pH values support very similar binding modes with the HAHH and HAHAH ligands. Above pH 8.3, however, the aquired spectra for these two systems are rather different (Fig. 6/B) indicating significant change in the structure of the corresponding metal complexes with the two peptides. While for the HAHH on increasing the pH an increase of the intensity of the band at 385 nm can be seen for HAHAH decrease and a parallel hypsochromic shift is observable (Fig. 6/B).

Fig. 6

To provide further proof on the composition of the complexes, mass spectrometry was also used. The m/z values of the major species present in solution at various pH values are summarized in Table 3. All the detected ions in Table 3 were also simulated and an excellent agreement was found regarding observed and calculated isotope patterns and m/z values. As a representative example, MS spectrum of the $[(\eta^6\text{-}p\text{-cym})Ru(H_2O)_3]^{2+}$–HAHH system at 1:1 ratio and at pH = 6.5 is shown in Fig. 7. It can be seen that, beside $[ML]^{2+}$ with an m/z value of 388.630 (its simulation is presented in Fig. 8), another species with high intensity at 776.257 m/z is detectable. This second one corresponds to a complex with monopositive charge and one hydrogen less than $[ML]^{2+}$. These findings can be rationalized by assuming that in the latter species deprotonation and coordination of one of the amide nitrogens occurs (formation of a mixed hydroxido species with $[ML(OH)]^+$ stoichiometry would result in a m/z value of 792 but this is not detectable in measureable concentration in the spectra). In contrast with the CD information obtained in the basic pH range, identical behaviour of the $[(\eta^6\text{-}p\text{-cym})Ru(H_2O)_3]^{2+}$–HAHH and –HAHAH systems was found by MS. In particular, increasing hydrolysis resulting in the formation of $[\{(\eta^6\text{-}p\text{-cym})Ru\}_2(\mu^2\text{-}OH)_3]^+$ (523.038 m/z) and parallel formation of $[MLH_{-1}]^+$ or $[MLH_{-2}]$ type species (Table 3) are detected.

Table 3

Fig. 7

Fig. 8

Since the imidazole side chain of the His residue can in principle coordinate to a given metal ion at elevated pH via both of the *N1* and *N3* donors (due to tautomerization) it was also interesting to study what is the donor atom preference for these half-sandwich type Ru(II) complexes. Inspired by literature data on the ^{13}C NMR behaviour of the square planar binding

isomers in the Pd(II)-Ac-HAAAH-NH$_2$ system [19] we have also undertaken the ^{13}C NMR study of the [(η^6-*p*-cym)Ru(H$_2$O)$_3$]$^{2+}$–HAHH, and –HAHAH systems to clarify the most likely (*N1* vs. *N3*) binding mode of the imidazole units. Based on the spectra, as it was detailed in the Introduction, the $\Delta\delta$ values for the [ML]$^{2+}$ complexes in these systems were calculated. As it is also indicated in Fig. 9, the positive $\Delta\delta$ for the C5 and the negative $\Delta\delta$ value for the C4 carbons in our systems show identical trend with those obtained for the (*N1,N1*) binding isomer of the Pd(II)–HAAAH system and, therefore, strongly supports the identical *N1* coordination of imidazolyl moieties of the ligands in the [ML]$^{2+}$ complexes with both HAHH and HAHAH.

Fig. 9

In order to obtain further proof on this binding mode a model pentapeptide, Ac-H*AH*AH*-NH$_2$ with three *N3*-methylated His units was also synthesized and its binding to [(η^6-*p*-cym)Ru(H$_2$O)$_3$]$^{2+}$ was studied. MS results were consistent again with the formation of [ML]$^{2+}$ (obs.: 445.173, calcd.: 445.174 m/z) as major species at pH ~ 7.4 with this ligand too. Furthermore, based on the ^{13}C NMR data, the calculated $\Delta\delta$ values showed an identical trend in their sign as for the non-methylated oligopeptides, HAHH and HAHAH (Fig. 9), providing thus clear evidence for the identical (*N1, N1, N1*) coordination mode.

3.3. DFT results

Over the last years, DFT methods were used with good results to calculate the relative stability of several metal complexes (see Section 2.3). In this study, the solvent (H$_2$O) effect was simulated using the SMD model, based on the quantum mechanical charge density of a solute molecule interacting with a continuum description of the solvent; this model has been demonstrated to give good results in the prediction of solvation free energy [37]. In particular, two the conformers of ML (L = Ac-HAHAH-NH$_2$ indicated with ML^1 and ML^2, with a different orientation of the isopropyl and methyl substituents on benzene) [49] and two coordinations of His residues (through *N1* and *N3* nitrogen donors) were examined: ML^1(*N1*), ML^1(*N3*), ML^2(*N1*) and ML^2(*N3*), see Fig. S6.

The geometry of the four species was optimized considering the relativistic effects due to the presence of a heavy atom such as Ru. The most popular approximation to account for these effects is the pseudo-potential or effective core potential (ECP) approach, where the innermost electrons are not treated explicitly but subsumed into a specially designed, mean

potential acting upon the outer electrons. Recently, this approximation was used to predict the geometry of the complexes formed by second-row transition-metal ions [32,50-52]; it has been shown that the use of ECP with the valence basis sets SDD (the Stuttgart-Dresden ECP) [35] and LANL2DZ [36] on the metal gives good results in the geometry optimisation [32,50-52]. Among the functionals, hybrid ones are shown to be superior to GGAs and meta-GGAs, and B3P86 is highly recommended [50].

The relative stability of the four species was determined in terms of the value of ΔG^{tot}_{aq} for the reactions (1)-(3):

$$ML^1(NI) \rightleftarrows ML^2(NI) \tag{1}$$

$$ML^1(NI) \rightleftarrows ML^1(N3) \tag{2}$$

$$ML^1(NI) \rightleftarrows ML^2(N3) \tag{3}$$

The value of ΔG^{tot}_{aq} can be separated into three parts: the electronic plus nuclear repulsion energy (ΔE^{ele}), the thermal contribution (ΔG^{therm}) and the solvation free energy ($\Delta(\Delta G^{solv})$), as given in eq. (4). The thermal contribution was estimated using the ideal gas model and the calculated harmonic vibrational frequencies to determine the correction due to zero point energy (ZPE) and to thermal population of the vibrational levels:

$$\Delta G^{tot}_{aq} = \Delta E^{ele} + \Delta G^{therm} + \Delta(\Delta G^{solv}) \tag{4}$$

The Gibbs free energy in the gas phase (ΔG^{tot}_{gas}), instead, can be found by neglecting the term ($\Delta(\Delta G^{solv})$):

$$\Delta G^{tot}_{gas} = \Delta E^{ele} + \Delta G^{therm} \tag{5}$$

DFT methods indicate that the two conformers with coordination of NI, $ML^1(NI)$ and $ML^2(NI)$, are the most stable. The difference of free energy is very small, 5.7 kJ/mol. In contrast, the isomer with Ru binding by $N3$ donor, ML($N3$), is significantly less stable, and almost 240 kJ/mol separates it from ML(NI). An examination of the data in Table 4 indicates that the value of ΔG^{tot}_{gas} (in the range 325-330 kJ/mol) favours ML(NI) over ML($N3$); the more favorable ΔG^{solv} for ML($N3$) (89-93 kJ/mol) is not enough to compensate the value of ΔG^{tot}_{gas}.

The reason of this result resides in a higher intrinsic stability of ML(NI) than ML($N3$). The coordination of NI results in a more relaxed structure with an optimal value of the Ru–N distances, Ct–Ru–N and N–Ru–N angles, where Ct is centroid of the arene ligand (Table 5).

The optimized structures of the most stable conformers of ML(*N1*) (Fig. 10) and ML(*N3*) are shown in Fig. S7.

Fig. 10

    Similar DFT calculations were also carried out on the ML complex with Ac-HAHH-NH$_2$. Since for the pentapeptide a very small energy difference for ML^1 and ML^2 (regarding the position of the isopropyl and methyl groups of the benzene ring to the coordinating ligand) was found with the tetrapeptide only the *N1 vs*. *N3* coordination of the imidazoles of the ligand was studied. Considering eq. (2), the results in Table 4 clearly support the preference of *N1* coordination of this ligand too in the optimized structure. The calculated bond lengths and angles for both systems are summarized in Table 5.

Table 4

Table 5

4. Conclusions

Results of this study indicate that terminally protected oligopeptides containing three histidyl side chains are efficient binders of $[(\eta^6\text{-}p\text{-cym})Ru(H_2O)_3]^{2+}$, a model cation for studying biotransformation reactions of half-sandwich type organometallic complexes with antiproliferative potential. Although the rather slow complex formation processes in these systems prevented the estimation of stability constants for the various species present in aqueous solution the results of the combined use of NMR, MS and CD techniques are consistent with the formation of 1:1 $[(\eta^6\text{-}p\text{-cym})RuL]^{2+}$ (L = oligopeptide) type complexes as major species under biologically relevant conditions. (N$_{Im}$, N$_{Im}$, N$_{Im}$) binding mode of both HAHH and HAHAH in $[(\eta^6\text{-}p\text{-cym})RuL]^{2+}$ is evidenced from the NMR and MS results. Both comparative NMR and DFT results support the *N1* over *N3* coordination of the imidazole rings of the ligands to the metal ion. On coordination of the ligands having the imidazole N donors in different chemical environment the metal ion also becomes a stereogenic center beside the α-carbon atoms of the L-amino acid building blocks. Monitoring the CD activity of samples with 1:1 metal ion to ligand ratio in the range 2.0 < pH < 8.0 reveals almost identical behaviour both with HAHH and HAHAH. This suggests that in the physiological pH range the position of the histidyl residues in the sequence has little effect on the stability of the [ML]$^{2+}$ complexes with ($N1_{Im}$, $N1_{Im}$, $N1_{Im}$) binding mode. In the more basic pH range, however, the different CD spectra suggest different binding mode and/or arrangement of the two ligands in the appropriate half-sandwich complexes and this might be connected to the

14

position of the His moieties in the peptides. Namely, in HAHH it is more likely that the peptide bond between the adjacent His residues becomes a metal ion binding site than for HAHAH. To understand fully this behaviour further studies are in progress in our laboratories.

Abbreviations

A, Ala – L-alanyl
AcOH – acetic acid
CD – circular dichroism
COSY – correlation spectroscopy
DCM – dichloromethane
DFT – density functional theory
DIPEA – N,N-diisopropyl-ethylamine
DMF – N,N-dimethylformamide
DODT – 3,6-dioxa-1,8-octanedithiol
ESI-TOF-MS – electrospray ionization time-of-flight mass spectrometry
Fmoc – N-fluorenylmethoxycarbonyl
H, His – L-histidyl
H*, His* – *N3*-methylated histidyl, His(*N3*-Me)
HHH – Ac-His-His-His-NH$_2$
HAHH – Ac-His-Ala-His-His-NH$_2$
HAHAH – Ac-His-Ala-His-Ala-His-NH$_2$
H*AH*AH* – Ac-His(*N3*-Me)-Ala-His(*N3*-Me)-Ala-His(*N3*-Me)-NH$_2$
HMBC – heteronuclear multiple-bond correlation
HOBt·H$_2$O – 1-hydroxybenzotriazole hydrate
HSQC – heteronuclear single quantum coherence
Im – imidazole
NMP – N-methyl-pyrrolidone
p-cym – 1-methyl-4-isopropylbenzene, *p*-cymene
R$_t$ – retention time
RP-HPLC – reversed-phase high-performance liquid chromatography
TBTU – 2-(1-H-benzotriazole-1-yl)-1,1,3,3-tetramethyluronium tetrafluoroborate
TIS – triisopropylsilane
TFA – trifluoroacetic acid

Acknowledgement

References

1. H. Kozłowski, W. Bal, M. Dyba, T. Kowalik-Jankowska, Coord. Chem. Rev. 184, 1 (1999) 319–346.
2. A.R. Timerbaev, C.G. Hartinger, S.S. Aleksenko, B.K. Keppler, Chem. Rev. 106, (2006) 2224–2248.
3. R.J. Sundberg, R.B. Martin, Chem. Rev. 74, 4 (1974) 471–517.
4. W.S. Sheldrick, R. Exner, Inorg. Chim. Acta 195, 1 (1992) 1–9.
5. D. Lazic, A. Arsenijevic, R. Puchta, Z.D. Bugarcic, A. Rilak, Dalton Trans. 45, 11 (2016) 4633–4646.
6. L. Messori, F.G. Vilchez, R. Vilaplana, F. Piccioli, E. Alessio, B. Keppler, Metal Based Drugs 7, 6 (2000) 335–342.
7. F. Wang, J. Bella, J.A. Parkinson, P.J. Sadler, J. Biol. Inorg. Chem. 10, 2 (2005) 147–155.
8. M. Hahn, D. Wolters, W.S. Sheldrick, F.B. Hulsbergen, J. Reedijk, J. Biol. Inorg. Chem. 4, 4 (1999) 412–420.
9. A. Muheim, R.J. Todd, D.R. Casimiro, H.B. Gray, F.H. Arnold, J. Am. Chem. Soc. 115, 12 (1993) 5312–5313.
10. R.S. Herrick, C.J. Ziegler, T.C. Leeper, J. Organomet. Chem. 751 (2014) 90–110.
11. I.W. Mcnae, K. Fishburne, A. Habtemariam, T.M. Hunter, M. Melchart, F. Wang, M.D. Walkinshaw, P.J. Sadler, Chem. Commun. 16 (2004) 1786–1787.
12. Z. Bihari, Z. Nagy, P. Buglyó, J. Organomet. Chem. 782 (2015) 82–88.
13. I. Sóvágó, K. Várnagy, N. Lihi, Á. Grenács, Coord. Chem. Rev. (2016) DOI: 10.1016/j.ccr.2016.04.015.
14. P. Tsiveriotis, N. Hadjiliadis, Coord. Chem. Rev. 190-192 (1999) 171–184.
15. P. Tsiveriotis, N. Hadjiliadis, G. Stavropoulos, Inorg. Chim. Acta 261, 1 (1997) 83–92.
16. M.T. Ma, H.N. Hoang, C.C. Scully, T.G. Appleton, D.P. Fairlie, J. Am. Chem. Soc. 131, 12 (2009) 4505–4512.
17. M.J. Kelso, H.N. Hoang, T.G. Appleton, D.P. Fairlie, J. Am. Chem. Soc. 122, 42 (2000) 10488–10489.
18. J.P. Snyder, A.S. Lakdawala, M.J. Kelso, J. Am. Chem. Soc. 125, 3 (2003) 632–633.
19. H.N. Hoang, G.K. Bryant, M.J. Kelso, R.L. Beyer, T.G. Appleton, D.P. Fairlie, Inorg. Chem. 47, 20 (2008) 9439–9449.
20. J. Baker, M.F. Ho, A. Pelecanos, M. Gatton, N. Chen, S. Abdullah, A. Albertini, F. Ariey, J. Barnwell, D. Bell, J. Cunningham, D. Djalle, D.F. Echeverry, D. Gamboa, J. Hii, M.P. Kyaw, J. Luchavez, C. Membi, D. Menard, C. Murillo, S. Nhem, B. Ogutu, P. Onyor, W. Oyibo, S.Q. Wang, J. McCarthy, Q. Cheng, Malaria J. 9 (2010) 129-140.
21. C. Brenner, P. Bieganowski, H.C. Pace, K. Huebner, J. Cell Physiol. 181, 2 (1999) 179–187.
22. D.D. Perrin, W.L.F. Armarego, Purification of Laboratory Chemicals, 3rd ed., Pergamon, Oxford, (1988).
23. M.A. Bennett, A.K. Smith, J. Chem. Soc., Dalton Trans. 2 (1974) 233–241.
24. A.J. Godó, A.C. Bényei, B. Duff, D.A. Egan, P. Buglyó, RSC Adv. 2, 4 (2012) 1486–1495.
25. G. Gran, Acta Chem. Scand. 4 (1950) 559–577.
26. H.M. Irving, M.G. Miles, L.D. Pettit, Anal. Chim. Acta 38 (1967) 475–488.
27. L. Zékány, I. Nagypál „Computational Methods for the Determination of Stability Constants" in Computational Methods for the Determination of Formation Constants, ed.: D.J. Leggett, Plenum Press, New York, USA (1985) 291–299.
28. P. Gans, A. Sabatini, A. Vacca, J. Chem. Soc., Dalton Trans. 6 (1985) 1195–1200.

29. L. Bíró, E. Farkas, P. Buglyó, Dalton Trans. 41, 1 (2012) 285–291.

30. A. Krężel, W. Bal, J. Inorg. Biochem. 98, 1 (2004) 161–166.

31. M.J. Frisch, G.W. Trucks, H.B. Schlegel, G.E. Scuseria, M.A. Robb, J.R. Cheeseman, G. Scalmani, V. Barone, B. Mennucci, G.A. Petersson, H. Nakatsuji, M. Caricato, X. Li, H.P. Hratchian, A.F. Izmaylov, J. Bloino, G. Zheng, J.L. Sonnenberg, M. Hada, M. Ehara, K. Toyota, R. Fukuda, J. Hasegawa, M. Ishida, T. Nakajima, Y. Honda, O. Kitao, H. Nakai, T. Vreven, J.A. Montgomery, Jr. J.E. Peralta, F. Ogliaro, M. Bearpark, J.J. Heyd, E. Brothers, K.N. Kudin, V.N. Staroverov, R. Kobayashi, J. Normand, K. Raghavachari, A. Rendell, J.C. Burant, S.S. Iyengar, J. Tomasi, M. Cossi, N. Rega, J.M. Millam, M. Klene, J.E. Knox, J.B. Cross, V. Bakken, C. Adamo, J. Jaramillo, R. Gomperts, R.E. Stratmann, O. Yazyev, A.J. Austin, R. Cammi, C. Pomelli, J.W. Ochterski, R.L. Martin, K. Morokuma, V.G. Zakrzewski, G.A. Voth, P. Salvador, J.J. Dannenberg, S. Dapprich, A.D. Daniels, Ö. Farkas, J.B. Foresman, J.V. Ortiz, J. Cioslowski, D.J. Fox „Gaussian 09, revision C.01" Gaussian, Inc., Wallingford, CT, (2009).

32. M. Bühl, C. Reimann, D.A. Pantazis, T. Bredow, F. Neese, J. Chem. Theory Comput. 4, 9 (2008) 1449–1459.

33. G. Micera, E. Garribba, Internat. J. Quant. Chem. 112, 12 (2012) 2486–2498.

34. L. Bíró, A.J. Godó, Z. Bihari, E. Garribba, P. Buglyó, Eur. J. Inorg. Chem. 2013, 17 (2013) 3090–3100.

35. M. Dolg; U. Wedig; H. Stoll, H. Preuss, J. Chem. Phys. 86, 2 (1987) 866–872.

36. P.J. Hay, W.R. Wadt, J. Chem. Phys. 82, 1 (1985) 299–310.

37. A.V. Marenich, C.J. Cramer, D.G. Truhlar, J. Phys. Chem. B. 113, 18 (2009) 6378–6396.

38. D. Sanna, K. Várnagy, S. Timári, G. Micera, E. Garribba, Inorg. Chem. 50, 20 (2011) 10328–10341.

39. D. Sanna, P. Buglyó, L. Bíró, G. Micera, E. Garribba, Eur. J. Inorg. Chem. 2012, 7 (2012) 1079–1092.

40. D. Sanna, P. Buglyó, A.I. Tomaz, J.C. Pessoa, S. Borovic; G. Micera, E. Garribba, Dalton Trans. 41, 41 (2012) 12824–12838.

41. L. Pisano, K. Várnagy, S. Timári, K. Hegetschweiler, G. Micera, E. Garribba, Inorg. Chem. 52, 9 (2013) 5260–5272.

42. D. Sanna, K. Várnagy, N. Lihi, G. Micera, E. Garribba, Inorg. Chem. 52, 14 (2013) 8202–8213.

43. Cs. Kállay, K. Várnagy, G. Malandrinos, N. Hadjiliadis, D. Sanna, I. Sóvágó, Inorg. Chim. Acta 362 (2009) 935-945.

44. K. Severin, R. Bergs, W. Beck, Angew. Chem. Int. Ed. 37 (1998) 1634–1654.

45. F.A. Egbewande, L.E.H. Paul, B. Therrien, J. Furrer, Eur. J. Inorg. Chem. 2014 (2014) 1174-1184.

46. W.S. Sheldrick, E. Hauck, S. Korn, J. Organomet. Chem. 467 (1994) 283–292.

47. R. Krämer, K. Polborn, H. Wanjek, I. Zahn, W. Beck, Chem. Ber 123 (1990) 767-778.

48. H. Brunner, Angew. Chem. Int. Ed. 38 (1999) 1194-1208.

49. N. Komiya, T. Nakajima, M. Hotta, T. Maeda, T. Matsuoka, S. Kawamorita, T. Naota, Eur. J. Inorg. Chem. 19 (2016) 3148–3156.

50. M. Bühl, H. Kabrede, J. Chem. Theory Comput. 2, 5 (2006) 1282–1290.

51. M.P. Waller, H. Braun, N. Hojdis, M. Bühl, J. Chem. Theory Comput. 3, 6 (2007) 2234–2242.

52. P. Comba, M. Kerscher, Coord. Chem. Rev. 253, 5–6 (2009) 564–574.

Table 1. Overal protonation ($\log\beta$) and stepwise deprotonation (pK) constants of histidine-containing oligopeptides at 25.0 °C and I = 0.20 M KNO$_3$.

	Ac-HHH-NH$_2$	Ac-HAHH-NH$_2$	Ac-HAHAH-NH$_2$
$[HL]^+$	6.95(1)	6.94(1)	7.02(1)
$[H_2L]^{2+}$	13.27(1)	13.28(1)	13.35(1)
$[H_3L]^{3+}$	18.88(1)	18.99(1)	19.15(1)
pK_1	5.61	5.71	5.80
pK_2	6.32	6.34	6.33
pK_3	6.95	6.94	7.02

Table 2. Chemical shift values (δ) assigned in the aromatic region for the ligands and the *p*-cymene unit of $[(\eta^6\text{-}p\text{-cym})Ru]^{2+}$ in free and complexed form at various pH values.

δ (ppm)	Ac-HAHH-NH$_2$			Ac-HAHAH-NH$_2$		
	Hϵ1	Hδ2	*p*-cymene	Hϵ1	Hδ2	*p*-cymene
uncomplexed pH = 2.0	8.61 8.61 8.61	7.29 7.29 7.28	5.73 5.98	8.69 8.69 8.68	7.33 7.32 7.30	5.73 5.98
uncomplexed pH = 11.0	7.65 7.64 7.63	6.91 6.88 6.87	5.17 5.38	7.65 7.64 7.64	6.94 6.91 6.90	5.17 5.38
complexed pH = 7.8	8.51 – 4.72 8.19 – 5.51 8.17 – 6.38		6.01 – 5.70 5.90 – 5.78	8.24 – 5.77 8.17 – 5.87 7.02 – 7.17		6.01 – 5.64 5.87 – 5.77

Table 3. Observed major cationic species in the $[(\eta^6\text{-}p\text{-cym})Ru(H_2O)_3]^{2+}$–peptide (L) systems together with their calculated m/z values given in parenthesis (A = Ala, H = His).

L = Ac-HAHH-NH$_2$

pH	2.18	2.84	5.72	8.59	10.3
$[(\eta^6\text{-}p\text{-cym})Ru(L)]^{2+}$		388.630 *(388.632)*			-
$[(\eta^6\text{-}p\text{-cym})Ru(LH_{-1})]^{+}$	-	-	776.255 *(776.257)*		
$[(\eta^6\text{-}p\text{-cym})Ru(LH_{-2})] + K^{+}$	-	-	-	814.213 *(814.213)*	
$[\{(\eta^6\text{-}p\text{-cym})Ru\}_2(\mu^2\text{-OH})_3]^{+}$	-	-	-	523.038 *(523.037)*	

L = Ac-HAHAH-NH$_2$

pH	1.98	3.36	6.47	8.95	10.9
$[(\eta^6\text{-}p\text{-cym})Ru(L)]^{2+}$	-	424.152 *(424.151)*			-
$[(\eta^6\text{-}p\text{-cym})Ru(LH_{-1})]^{+}$	-	-	847.294 *(847.294)*		-
$[(\eta^6\text{-}p\text{-cym})Ru(LH_{-2})] + 2K^{+}$	-	-	-	462.104 *(462.108)*	
$[(\eta^6\text{-}p\text{-cym})Ru(LH_{-2})] + K^{+}$	-	-	-	885.247 *(885.250)*	
$[\{(\eta^6\text{-}p\text{-cym})Ru\}_2(\mu^2\text{-OH})_3]^{+}$	-	-	523.038 *(523.037)*		

Table 4. ΔG^{tot} values in the gas phase and in aqueous solution for the reaction of formation of the isomers $ML^2(N1)$, $ML^1(N3)$, $ML^2(N3)$ from $ML^1(N1)$.

Ligand / Reaction	ΔE^{ele}	$\Delta G^{therm\ b}$	ΔG^{tot}_{gas}	$\Delta(\Delta G^{solv})^{\ c}$	ΔG^{tot}_{aq}
L = Ac-**HAHAH**-NH$_2$					
$ML^1(N1) \rightleftarrows ML^2(N1)$	-1.0	4.0	3.0	2.7	5.7
$ML^1(N1) \rightleftarrows ML^1(N3)$	314.1	11.7	325.8	-89.3	236.5
$ML^1(N1) \rightleftarrows ML^2(N3)$	319.4	11.0	330.4	-93.2	237.2
L = Ac-**HAHH**-NH$_2$					
$ML^1(N1) \rightleftarrows ML^1(N3)$	247.5	8.1	255.6	-75.3	180.3

[a] All the values reported in kJ mol^{-1}. [b] Thermal contribution at 298 K with the zero-point energy included in the calculations. [c] SMD model used with water as the solvent. [d] M = $[(\eta^6\text{-}p\text{-cym})Ru]^{2+}$

Table 5. Optimized bond lengths (Å) and angles (°) for the most stable ML(*N1*) and ML(*N3*) isomers. M = [(η⁶-*p*-cym)Ru]²⁺, # Ct indicates the centroid of the arene ring.

Length / angle #	Ac-HAHH-NH$_2$		Ac-HAHAH-NH$_2$	
	ML(*N1*)	ML(*N3*)	**ML(*N1*)**	ML(*N3*)
Ru-N	**2.074**	2.107	**2.100**	2.149
	2.080	2.122	**2.123**	2.180
	2.091	2.232	**2.126**	2.222
Ru-C	**2.259-2.318**	2.258-2.461	**2.216-2.263**	2.185-2.323
Ru-Ct	**1.767**	1.749	**1.723**	1.740
Ct-Ru-N	**123.3**	116.0	**124.8**	120.9
	130.1	123.0	**130.0**	121.2
	130.5	134.5	**130.9**	133.8
N-Ru-N	**83.2**	79.7	**79.5**	79.3
	86.3	88.9	**87.6**	81.4
	88.8	106.2	**88.7**	109.4
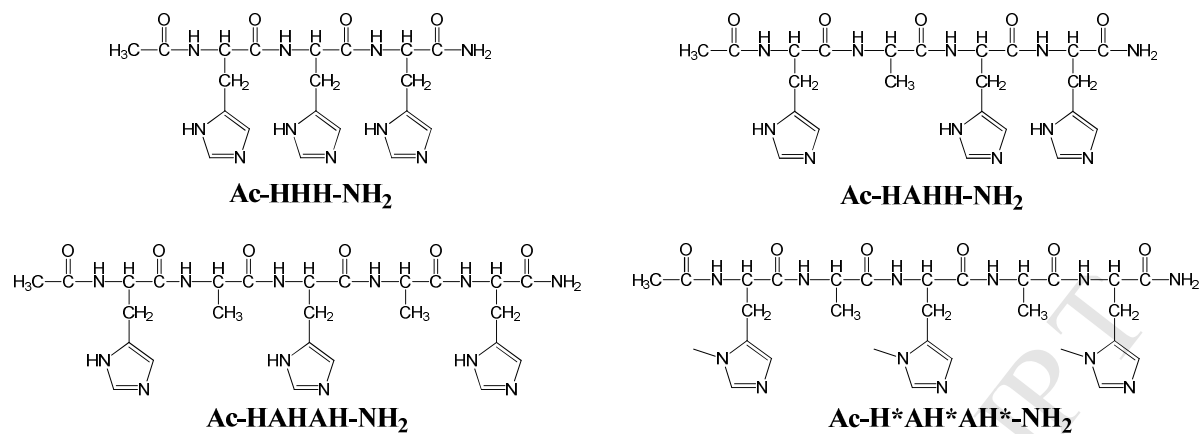
Figure 1. Structure of the neutral forms of the oligopeptides containing L-amino acids.
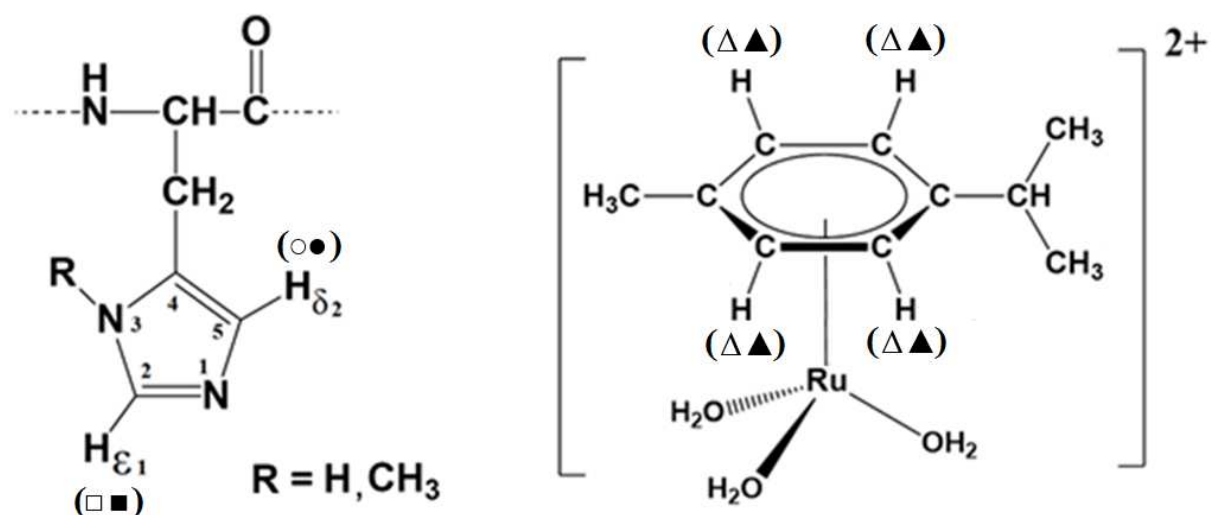
Scheme 1. Structure of the imidazole ring of the histidyl side chain and that of the $[(\eta^6\text{-}p\text{-}$cym)$Ru(H_2O)_3]^{2+}$ together with the labeling of the protons. In subsequent Figures resonances belonging to uncomplexed entities are marked with open while those of complexed ones with filled symbols.
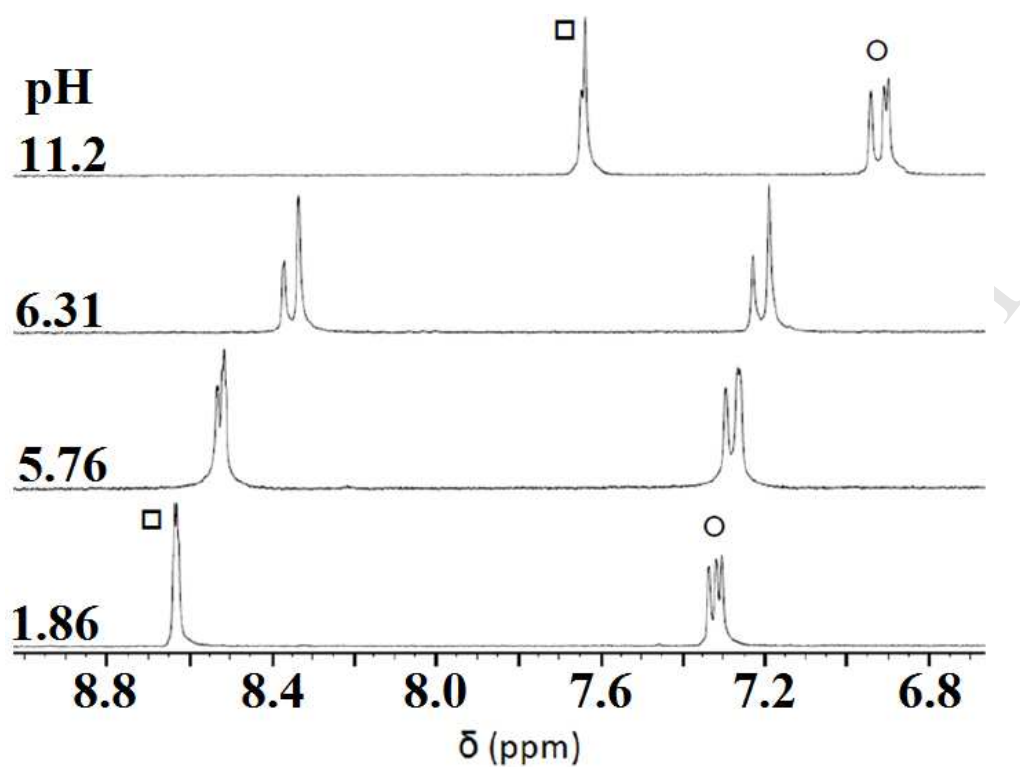
Figure 2. Dependence on pH of the low-field region of the ^{1}H NMR spectra of Ac-HAHAH-NH$_2$ at 298 K in D$_2$O (I = 0.20 M KNO$_3$). For notation of the hydrogens see Scheme 1.
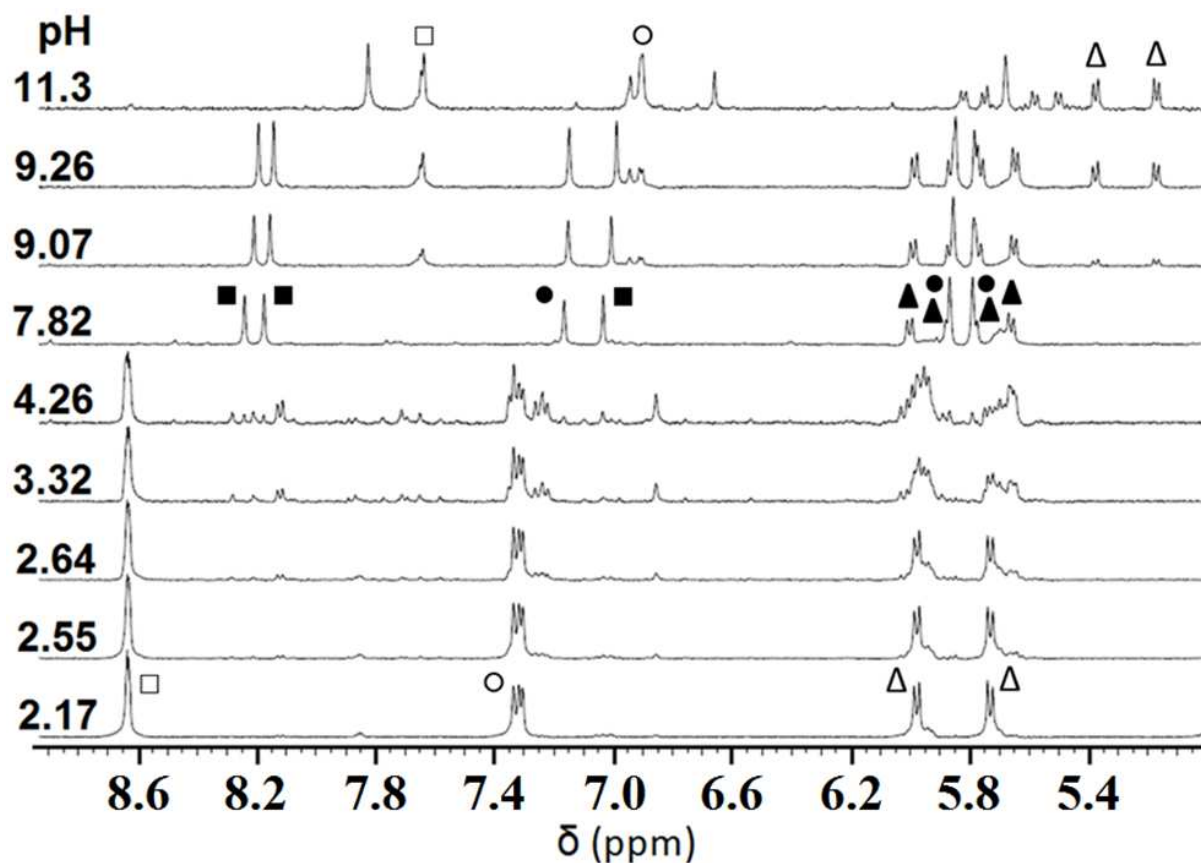
Figure 3. Dependence on pH of the low-field region of the ^{1}H NMR spectra of $[(\eta^6\text{-}p\text{-}$cym)Ru(H$_2$O)$_3]^{2+}$ – Ac-HAHAH-NH$_2$ system at 1:1 ratio in D$_2$O (T = 298 K, I = 0.20 M (KNO$_3$), c_{Ru} = 5.00 mM). For notation of the resonances see Scheme 1; resonances belonging to uncomplexed entities are marked with open while those of complexed ones with filled symbols.
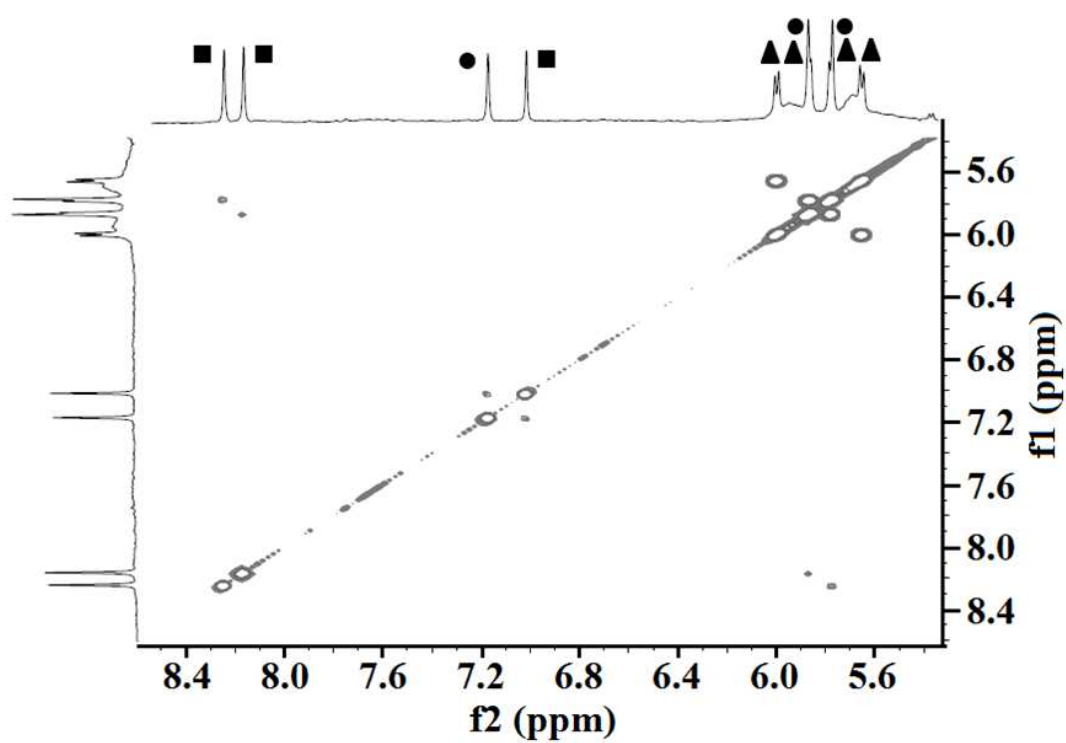
Figure 4. Low-field region of the ^{1}H-^{1}H COSY spectrum of [(η^6-p-cym)Ru(H$_2$O)$_3$]$^{2+}$ – Ac-HAHAH-NH$_2$ at pH = 7.82 in D$_2$O (T = 298 K, I = 0.20 M (KNO$_3$). For notation see Scheme 1.

Figure 5. Low-field region of the ^{1}H-^{13}C HSQC spectrum of $[(\eta^6$-p-cym)Ru(H$_2$O)$_3]^{2+}$ – Ac-HAHAH-NH$_2$ at pH = 7.82 in D$_2$O (T = 298 K, I = 0.20 M (KNO$_3$). For notation see Scheme 1.
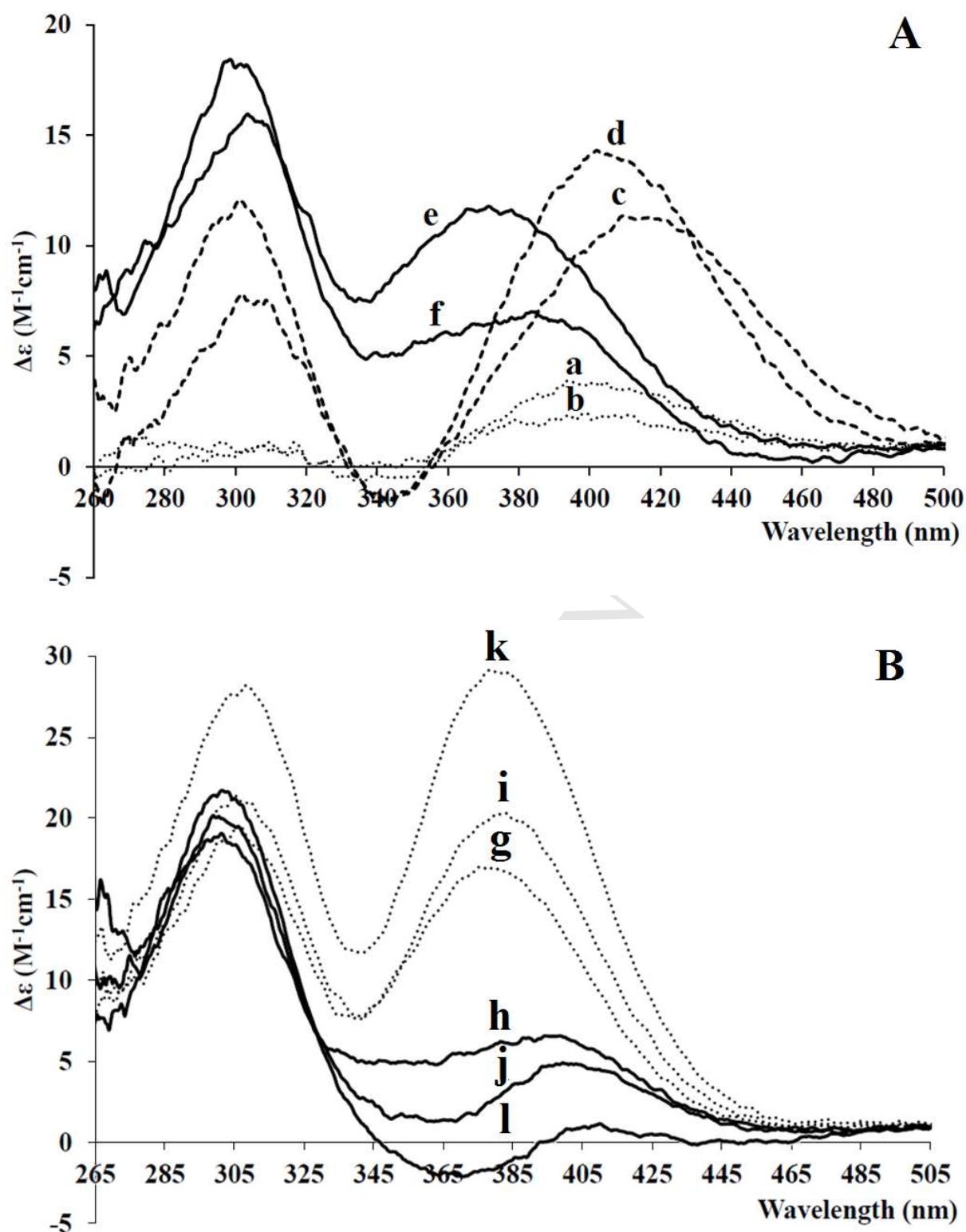
Figure 6. Effect of the increasing pH on the CD spectra of $[(\eta^6\text{-}p\text{-cym})Ru(H_2O)_3]^{2+}$ – Ac-HAHH-NH$_2$ (A, pH: a: 2.32; c: 3.74; e: 7.45) and $[(\eta^6\text{-}p\text{-cym})Ru(H_2O)_3]^{2+}$ – Ac-HAHAH-NH$_2$ (A, pH: b: 2.23; d: 3.91; f: 7.54) systems and $[(\eta^6\text{-}p\text{-cym})Ru(H_2O)_3]^{2+}$ – Ac-HAHH-NH$_2$ (B, pH: g: 8.31; i: 8.81; k: 9.68) and $[(\eta^6\text{-}p\text{-cym})Ru(H_2O)_3]^{2+}$ – Ac-HAHAH-NH$_2$ (B, pH: h: 8.49; j: 9.23; l: 10.2) systems in H$_2$O (T = 298 K).
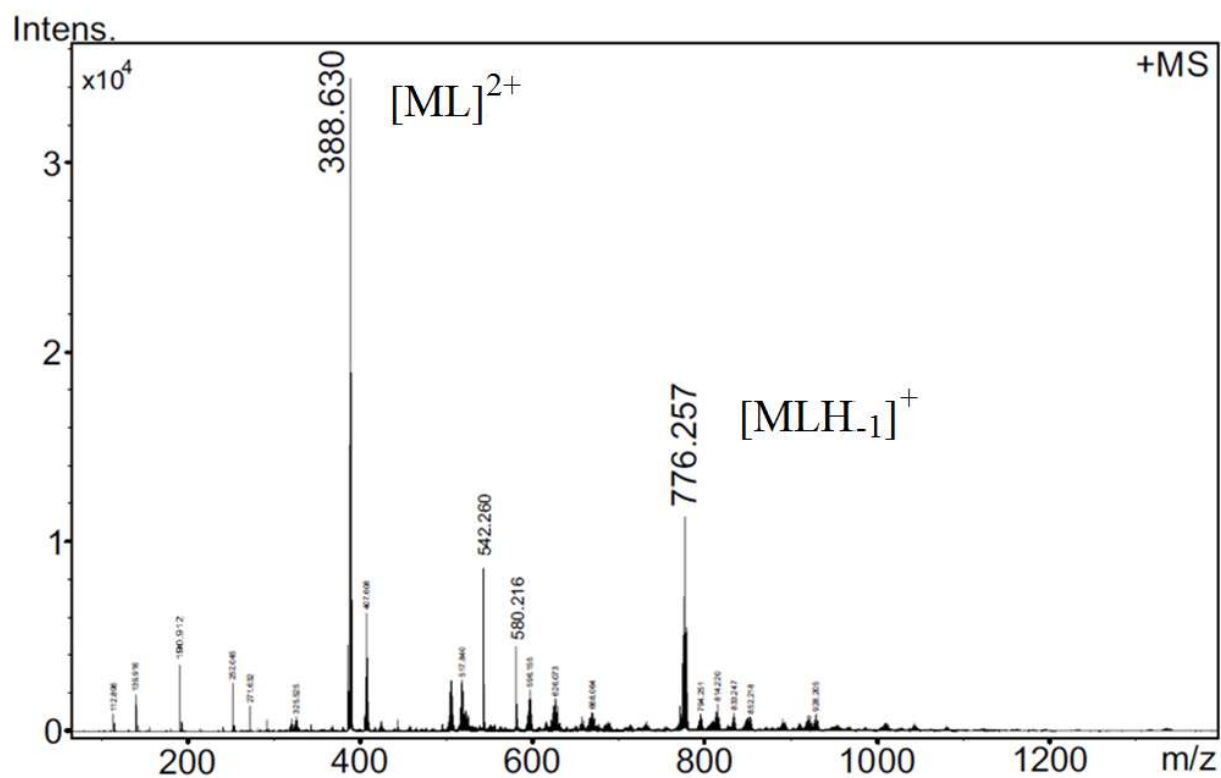
Figure 7. ESI-TOF-MS spectrum of the $[(\eta^6\text{-}p\text{-cym})Ru]^{2+}$ – Ac-HAHH-NH$_2$ system at 1:1 metal ion to ligand ratio, pH = 6.5.
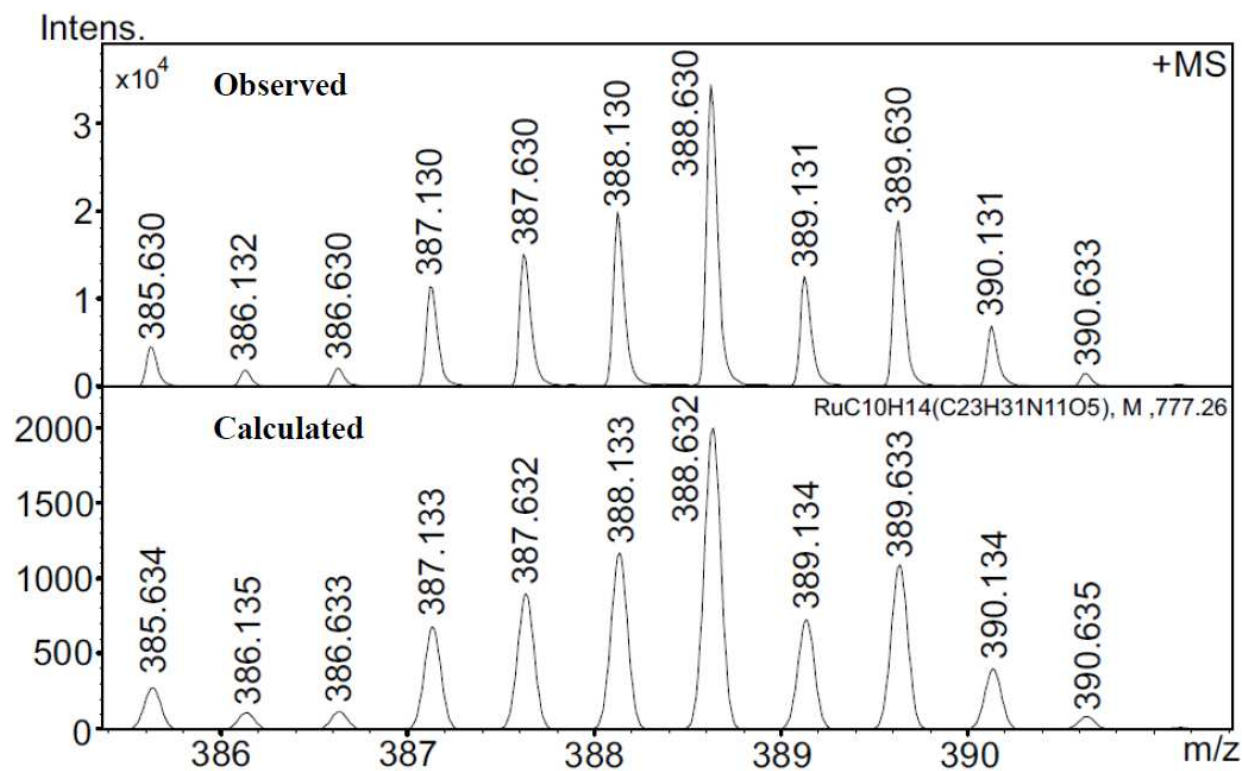
Figure 8. Representative observed and calculated ESI-TOF-MS spectra of $[ML]^{2+}$ complex, where M = $[(\eta^6\text{-}p\text{-cym})Ru]^{2+}$ and L = Ac-HAHH-NH$_2$.
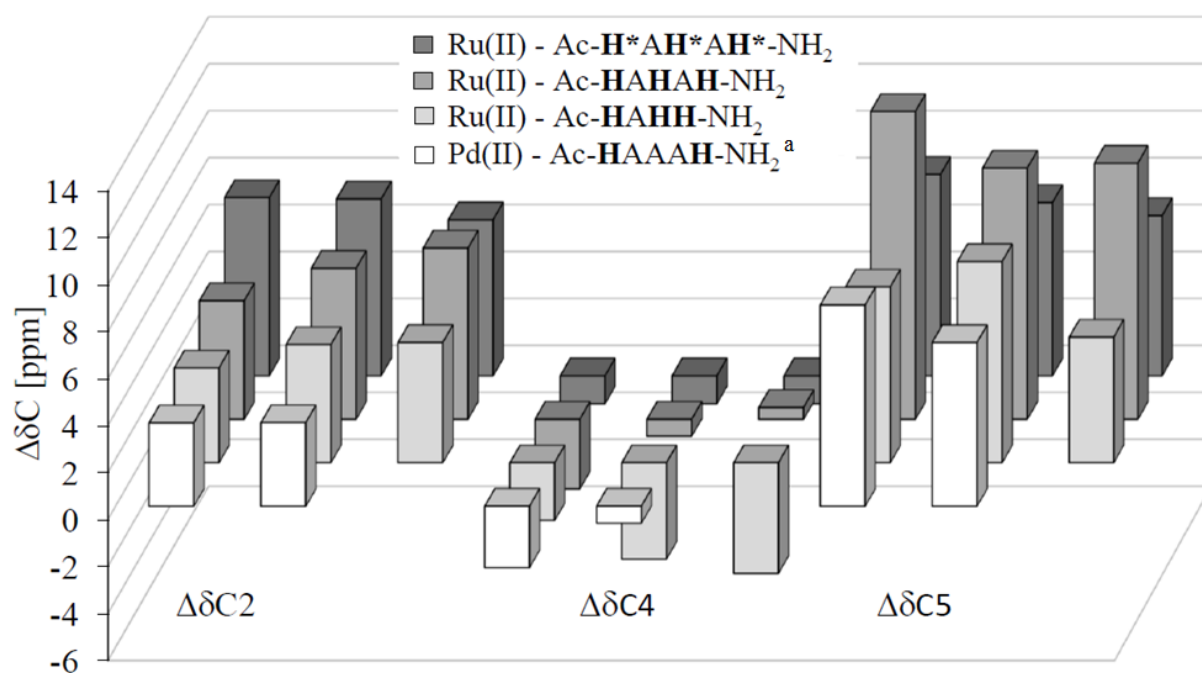
Figure 9. Deviation of chemical shifts of imidazole carbon atoms (C2, C4, C5) relative to those in the corresponding free peptide, $\Delta\delta = \delta C_{im}(complex) - \delta C_{im}(free\ peptide)$ in D_2O. [a]Taken from Ref. 18.
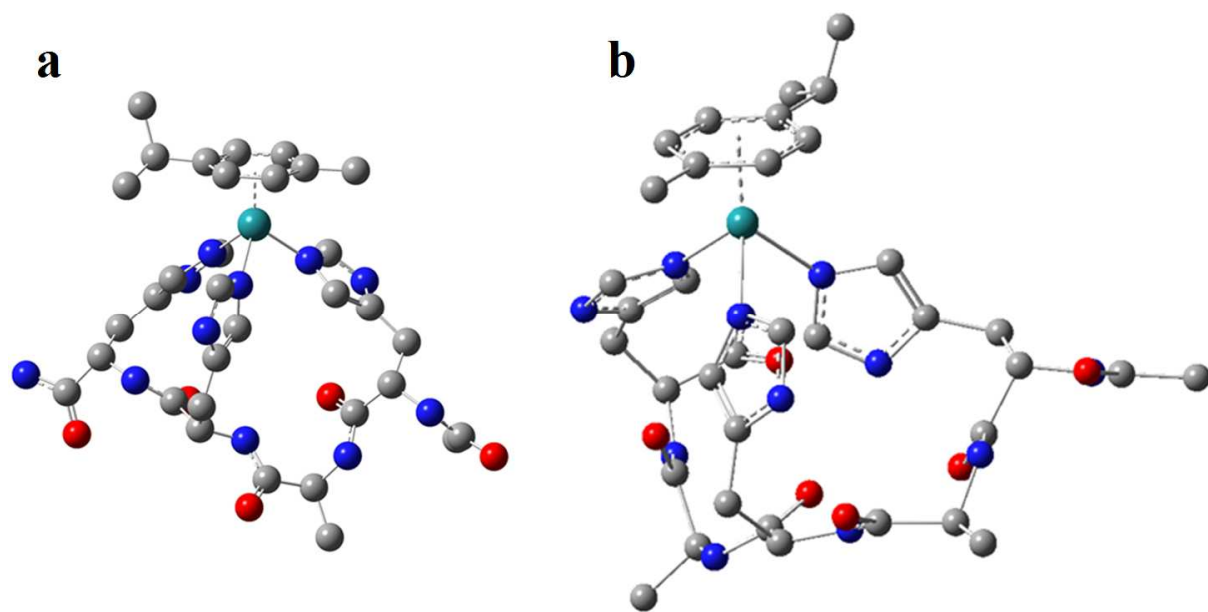
Figure 10. Optimized DFT structures of ML(*N1*) isomers, where L = Ac-HAHH-NH$_2$ (a) and L = Ac-HAHAH-NH$_2$ (b). Hydrogen atoms have been omitted for clarity.

- Solid-phase peptide synthesis of three histidine containing oligopeptides
- Solution equilibrium studies on the interaction between $[(\eta^6\text{-}p\text{-cym})Ru(H_2O)_3]^{2+}$ and the Ac-HAHH-NH$_2$ and Ac-HAHAH-NH$_2$ ligands
- Formation of (N$_{Im}$,N$_{Im}$,N$_{Im}$) coordinated 1:1 complexes with Ac-HAHH-NH$_2$ and Ac-HAHAH-NH$_2$
- DFT and NMR evidence for the *N1* over *N3* coordination of the imidazole moieties in the complexes